# O-X-B Mode Conversion in the TCV Tokamak

A.Mück[1], H.P.Laqua[2], S.Coda[1], B.P.Duval[1], T.P.Goodman[1], I.Klimanov[1], Y.Martin[1], A.Pochelon[1], L.Porte[1]

[1] *Association EURATOM- Confédération Suisse, EPFL SB CRPP, CH-1015 Lausanne*

[2] *Max-Planck-Institut für Plasmaphysik, Assoziation EURATOM, D-17491 Greifswald*

In high density tokamak plasmas, the accessibility of the plasma to electron cyclotron resonance heating (ECRH) is limited by so-called wave cut-offs. ECRH in extraordinary mode (X-mode) can not propagate to the plasma centre and heating in ordinary mode (O-mode) is prevented by the plasma cut-off at $\omega = \omega_{pe}$. At a particular launching angle, an O-mode wave converts to X-mode at the plasma cut-off. After this first mode conversion, the wave propagates back towards the plasma edge until it encounters the upper hybrid layer. There, a second mode conversion from X-wave into a Bernstein (B) wave, known as the O-X-B conversion, occurs. The Bernstein wave can propagate now to the plasma centre and may be absorbed at harmonics of the cyclotron resonance [1],[2].

In TCV, a high density H-mode scenario with up to $n_e \approx 2 \cdot 10^{20} \mathrm{m}^{-3}$ was developed to place the plasma ECH cut-off within the steep density gradient region at the H-mode discharge edge. The angular window of the O-X conversion is calculated with the power transmission function $T$ [3]

$$T(N_x, N_z) = exp\left(-\pi k_0 L \sqrt{\frac{1}{2\alpha}} \cdot \left[2(1 + \frac{1}{\alpha}(N_{z,opt} - N_z)^2 + N_x^2\right]\right) \quad (1)$$

which depends on the density scale length $L$ and the refraction indices $N_x$ and $N_z$. Only for the optimum $N_z$, equivalent to an optimum angle, can the O-mode wave be completely converted to X-mode.

In figure 1a), the main characteristics of such a H-mode discharge, as used in the reported experiments, is shown. High densities were achieved in non-stationary, but reproducible, discharges. Modulated O-mode ECRH at the second harmonic at 82.7 GHz and $P_{ECRH} \approx 470$ kW was injected with a low duty cycle to avoid ELM triggering. Poloidal and toroidal ECRH launcher angle scans were then performed on a shot by shot basis. In figure 1b), the change in the stray ECRH radiation signal of a midplane launcher from a diode located in sector 14 is shown. The same tendency in the signal is observed with a second diode in sector 9 and a sniffer probe in sector 2 (ECH is injected from sector 6 of TCV's 16 sectors). A clear dependence on the ECRH launcher angle is observed, shown in further detail in figure 2. In figure 2a) dots show the scan positions for a midplane launcher L4 for the injection angle calculated with the ART code [4]. In the figures 2b) and 2c) the stray radiation signal for the poloidal and toroidal angle scan are drawn separately as a function of the ECRH launcher angle. In these scans, as well as in scans with an upper lateral launcher, the angular dependence of the O-X conversion is clearly visible. The minimum in the stray radiation intensity, assumed to be the maximum of the ECRH power

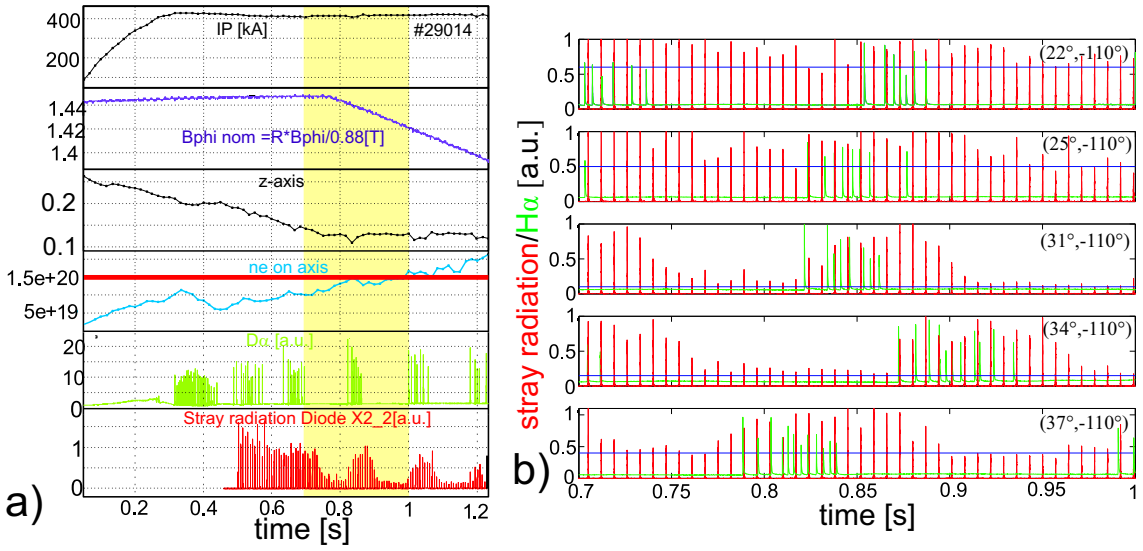


*Figure 1: a) Characteristics of developed high density H-mode discharge. b) ECRH stray radiation for different launching angles of the midplane launcher L4, showing an angle dependent behaviour and $D_\alpha$ signal, showing the influence of ELMs.*

absorption, varies of about $2^o$ from its predicted position, as shown in figure 2a).
Heating experiments were performed with a fixed poloidal launcher angle of $31^o$ and toroidal angle of -$107^o$ with a higher duty cycle. The correlation between the soft X-ray signal (DMPX) and the stray radiation signal was used to determine the deposition location. An anti-correlation

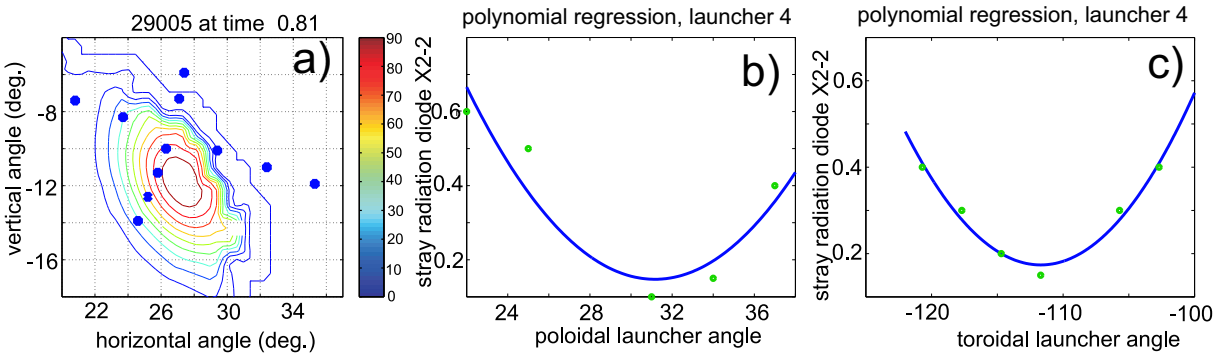


*Figure 2: a) ART simulation of angular window as transmission in percent. b) Poloidal angle scan with midplane launcher L4. c) Toroidal angle scan with L4.*

with the stray radiation signal $S_{stray}$ is expected from the inverse dependence of the stray radiation on the absorbed ECRH power. To obtain such a correlation, the value of the stray radiation signal without absorption $S_{stray,max} \approx 1.5$ was subtracted. To set a value of zero between the ECRH pulses, the signal was multiplied by the ECRH power time trace, leading to $C_{cross} = (S_{stray,max} - S_{stray}) \cdot P_{ECRH}$. By calculating the cross-correlation of one ECRH pulse across a sawtooth crash and within an ELM free time interval, clear localised deposition was found. Figure 3 shows the correlation for DMPX channels 22 ($\rho \approx -0.44$) and 47 ($\rho \approx 0.58$),

marked by a solid line. The ART calculated absorption is situated further in the plasma at $\rho \approx 0.35$ (channels 26, 42).

The calculated position of the plasma cut-off is marked by a dashed line. the ECRH power is reflected at the plasma cut-off and absorbed at the cyclotron resonance after reflection at the torus wall, explaining the correlation outside the cut-off. The amount of ECRH power absorbed is measured with the diamagnetic loop (DML). Figure 4a) shows an average absorbed power of 267 kW$\pm$12% ( 60%) with a phase below 90$^o$, confirming the reliability of the analysis together with figure 4b), which shows that the ECRH modulation frequency was well fitted in the DML signal. If O-X conversion does not take place, the maximum stray level rises to $S_{stray,max}$ 1.5. In the best case, a stray level of 0.15 is observed, indicating that an O-X coupling of up to 90% was achieved.

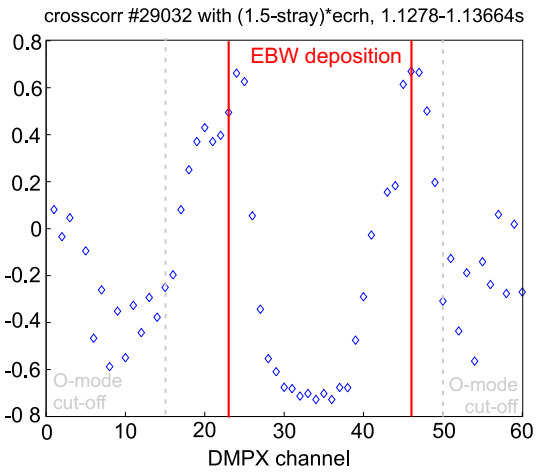


*Figure 3: Deposition location of #29032 at $B = 1.33$ T for ECRH pulse without sawtooth crash.*

The magnetic field dependence of the EBW deposition was investigated by increasing the toroidal field from $B = 1.33$T to $B = 1.39$T. In figures 5a) and 5b) the cross-correlation of $C_{cross}$ with the DMPX signal is shown for a sawtooth crash free and ELM free time period. The deposition locations of #29550 and #29565 are consistent with the ART simulation. No significant variation in the deposition location for $B = 1.33$ T and $B = 1.39$ T was however observed, as summarised in the table below . A possible explanation could be small changes in the edge current profile, strongly influencing the $k_{||}$ component of the converted Bernstein wave, leading to a change in

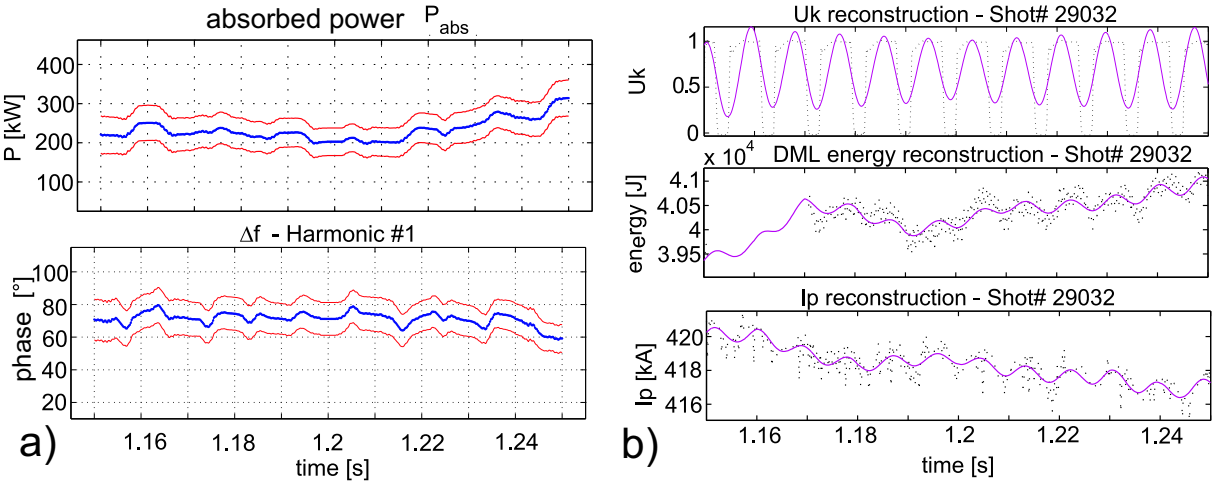


*Figure 4: a) Average deposited power and phase with iamagnetic loop. b) Fit of energy and current with ECRH frequency.*

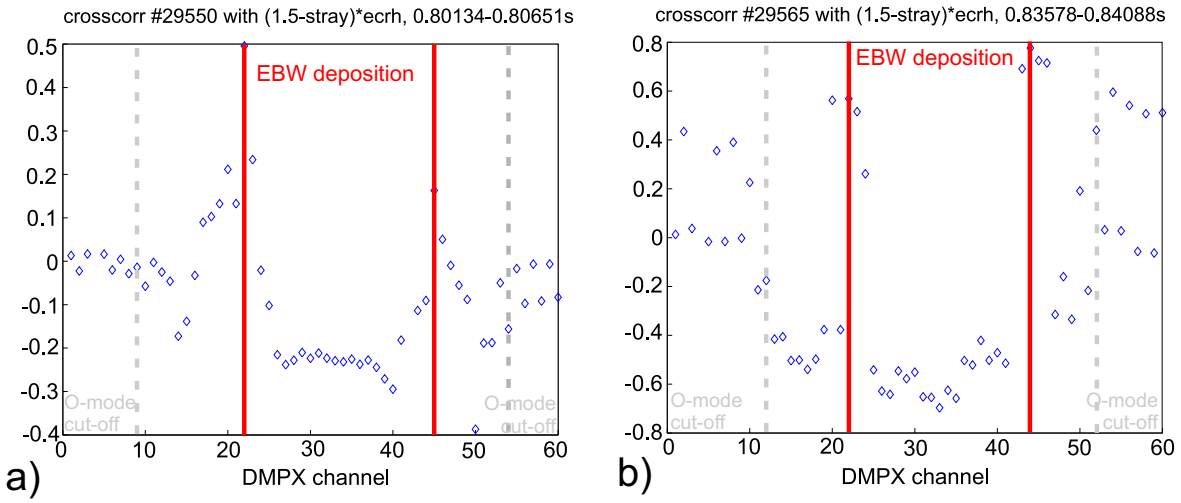


*Figure 5: Deposition location of a) #29550 and b) #29565 at $B = 1.39\ T$ for ECRH pulse without ELM and sawtooth crash.*

the wave propagation. These variations in the current may be in the range of the uncertainty in the equilibrium reconstruction.

| Shot | B field | O-X conversion | Absorption (ART) | Absorption (experiment) |
|---|---|---|---|---|
| #29032 | 1.33T | $\rho \sim 0.69$; ch 15, 50 | $\rho \sim 0.35$; ch 26, 42 | ch 22, 44 |
| #29550 | 1.39T | $\rho \sim 0.88$; ch 9, 54 | $\rho \sim 0.45$; ch 23, 44 | ch 22, 45 |
| #29565 | 1.39T | $\rho \sim 0.82$; ch 12, 54 | $\rho \sim 0.45$; ch 23, 44 | ch 22, 44 |

**Conclusions:**

For the first time in a standard aspect ratio tokamak, localised EBW deposition is demonstrated in overdense plasmas resulting from the O-X-B mode conversion process. Absorption of 60% of the injected ECRH power has been shown by DML measurements in heating experiments. In low power experiments, the stray radiation signal indicates an absorption even up to 90%. The angular dependence of the O-X conversion has been explored by scanning the ECRH launcher angles. The observed variation of the stray radiation signal is well confirmed by ART calculations of the angular window.

**References**

[1] I.Bernstein, Phys. Rev. Lett. **109**, 10 (1958)

[2] H.P.Laqua et al., Phys. Rev. Lett. **78**, 3467 (1997)

[3] E. Mjolhus et al., Plasma Phys. **31**, 7 (1984)

[4] F.Volpe, H.P.Laqua, Rev. Sci. Instrum. **74**, No. 3 (2003), pp. 1409-1413

*A. Mück is supported by a EURATOM fellowship.*